

Understanding voltage-controlled magnetic anisotropy effect for the manipulation of dipolar-dominated propagating spin waves

Adrien. A. D. Petrillo,¹ Mouad Fattouhi,² Adriano Di Pietro,^{3,4} Marta Alerany Solé,¹ Luis Lopez Diaz,² Gianfranco Durin,³ Bert Koopmans,¹ and Reinoud Lavrijsen¹

¹*Department of Applied Physics, Eindhoven University of Technology, Eindhoven, The Netherlands*

²*Departamento de Física Aplicada, Universidad de Salamanca, 37008 Salamanca, Spain*

³*Istituto Nazionale di Ricerca Metrologica, Strada delle Cacce 91, 10135, Torino, Italy*

⁴*Politecnico di Torino, Corso Duca degli Abruzzi 24, 10129, Torino, Italy*

(*Electronic mail: a.a.d.petrillo@tue.nl)

(Dated: 6 February 2024)

Spin waves, known for their ability to propagate without the involvement of moving charges, hold immense promise for on-chip information transfer and processing, offering a path toward post-CMOS computing technologies. This study investigates the potential synergy between propagating Damon-Eshbach spin waves and voltage-controlled magnetization in the pursuit of environmentally sustainable computing solutions. Employing micromagnetic simulations, we assess the feasibility of utilizing spin waves in DE mode in conjunction with localized voltage-induced alterations in surface anisotropy to enable low-energy logic operations. Our findings underscore the critical importance of selecting an optimal excitation frequency and gate width, which significantly influence the efficiency of the phase shift induced in propagating spin waves. Notably, we demonstrate that a realistic phase shift of $2.5[\pi \text{ mrad}]$ can be achieved at a Co(5nm)/MgO material system via the VCMA effect. Moreover, by tuning the excitation frequency, Co layer thickness, gate width, and the use of a GdO_x dielectric, we illustrate the potential to enhance the phase shift by a factor of 200 when compared to MgO dielectrics. This research contributes valuable insights towards developing next-generation computing technologies with reduced energy consumption.

The use of Magnonics in the context of wave-based computing has gained interest for its potential use as a low Ohmic-loss information carrier. Unlike conventional electronics, where information is conveyed through electronic charges, Magnonics employ spin-waves (SWs) to carry information through the amplitude and phase of a pseudo-particle known as a magnon. This innovative approach may open the road to beyond-CMOS computing technology¹⁻³ free of Joule heating. As data processing requires phase and amplitude modulation, novel ways of manipulating propagating SWs through a local change of the effective magnetic field have been explored, such as the application of a magnetic field⁴⁻⁶, local laser-induced heating⁷⁻⁹ or current¹⁰⁻¹². In particular, control of phase or amplitude by Oersted field or SW current has been a topic of study for the development of Mach-Zehnder spin-wave interferometer architecture¹³⁻¹⁵. In an effort to further decrease the energy consumption of magnetic materials-based computing devices, voltage-controlled magnetic anisotropy (VCMA) holds great promise, potentially reducing the energy consumption of storage and logic devices by a factor of 100¹⁶. Effects of an electric field on surface anisotropy (SA) have widely been studied over the recent years¹⁷⁻²⁵ and, in essence, can be used to manipulate the spin-wave (magnon) dispersion relation via two routes: a fast, volatile, electronic effect *e.g.*, direct solid-state gating, or a slow, non-volatile, magneto-ionic effect *e.g.*, moving mobile ions in or out of the ferromagnetic layers. The magneto-ionic effect is a process of electrochemical nature happening at ferromagnetic/oxide (FM/O) interfaces²⁶, where oxygen ions are brought to the interface between the oxide dielectric and the ferromagnetic layer. Due to coupling between 2p orbitals of oxygen ions and 3d orbitals from Co at the interface²⁷, changes in charge densities lead to a change of the magnetic anisotropy via a

modulated spin-orbit coupling. The magneto-electronic effect has been interpreted as a change of the electronic occupation state at the interface between the dielectric and the ferromagnetic layer²⁸⁻³⁰ and electric-field-induced dipole³¹. While volatile, the latter effect is particularly suited for logic due to the fast transport of the charges at the interface, compared to magneto-ionic effects befitting for storage devices due to their non-volatility but slower response due to the electrochemical nature.

Theoretical and experimental studies based on VCMA control of SWs include reconfigurable magnonic crystals³², nanochannels^{32,33} and SW phase shifters^{34,35}. Moreover, these studies have primarily been focusing on insulating ferromagnetic SW conduits of yttrium iron garnet (YIG)^{36,37}. In particular, studies have concentrated on the Damon-Eshbach (DE) SW mode configuration. Indeed, due to the localization of DE SWs at the interfaces of the ferromagnetic layer in direct contact with the dielectric where the VCMA effect is induced, the VCMA-induced non-reciprocal transport of the SWs can efficiently be probed using a phase-sensitive all-electrical method³⁸⁻⁴⁰. In these studies, the VCMA effect was assumed to be applied homogeneously along the entire spin-wave conduit. Hence, the question of what happens when the VCMA effect is applied locally along the path of a spin-wave conduit remains open.

In this study, we present an investigation of the impact of locally applied electric fields at the interface between a Co ferromagnetic layer and a MgO dielectric on dipole-dominated DE propagating SWs within thin-film SW-conduits, employing Mumax³ micromagnetic simulations⁴¹. Initially, we elucidate the influence of SA modifications on the dispersion characteristics of the excited modes, shedding light on their implications for the wavevector of SWs both entering and

exiting the VCMA-gated region. Subsequently, we examine the propagation characteristics of the resulting scattered SWs. Furthermore, we analyze the frequency and gate width-dependent VCMA-induced phase shifts in the scattered SWs at a local scale. Finally, we discuss the feasibility of employing the DE configuration for SW phase shifting with a metallic Cobalt ferromagnetic waveguide and optimizing the ferro-magnetic/dielectric interface.

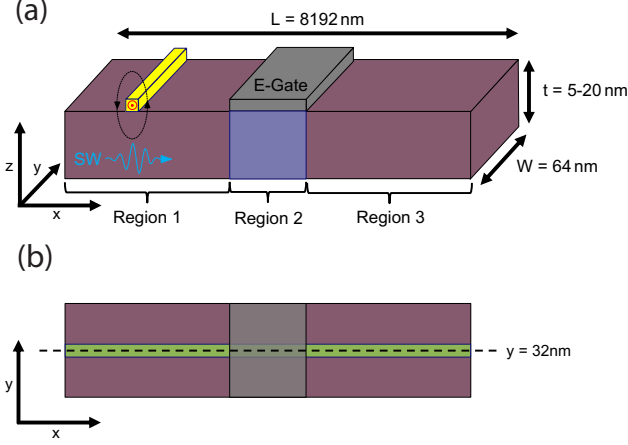


FIG. 1: (a) Schematic of the system under study. The strip is divided into three regions. The SW is excited in region 1, K_S is modified within region 2, under the gate, and the SW is detected in region 3. (b) Top view of the simulation box. A row of cells (in green) of $2 \times 2 \times 2.5$ nm centered around the center of the strip ($y=32$ nm) along which the magnetization is sampled.

Our model system is an 8192 nm long (x) and 64 nm (y) wide Co waveguide with a thickness of 5, 10, and 20 nm (z). The simulation box is subdivided in $2 \times 2 \times 2.5$ nm cells in the x -, y -, z - directions. Due to the narrowness of our waveguide and our focus on the lowest frequency DE mode i.e, the wavevector along (y) $k_y=0$, Periodic Boundary Conditions (PBCs) are applied along y . The used magnetic parameters for Cobalt are $\gamma = 1.9 \times 10^{11}$ Hz rad/T, $M_S = 1.42 \times 10^6$

A/m, $A_{ex} = 20 \times 10^{-12}$ J/m, and $\alpha = 0.005$ respectively, representing the gyro-magnetic ratio, the saturation magnetization, the exchange stiffness and the damping, respectively. No uniaxial anisotropy is introduced. Exponentially increasing spatial damping profiles over a distance of 1.016 μ m are introduced at both ends (x) of the simulation box to prevent SW reflections. DE SWs are excited by applying a static transverse magnetic field of 100 mT along y , fully saturating the magnetization in the y -direction and applying a sinusoidal AC magnetic field with a Gaussian profile varying in the x direction for a time period of $t = 10$ ns, leading to a spin-wave with small time-dependent dynamic magnetization components in the x - z plane.

In the following, we define three regions (See Fig. 1a). In region 1 and 3, the base anisotropy $K_{S_{E=0}} = 0.71 \times 10^{-3}$ J/m² is chosen following Kasukawa *et. al.*³⁸, with $E = 0$ indicating the nominal anisotropy of the waveguide, i.e., when no VCMA is applied. In region 2, we emulate the effect of VCMA, *e.g.*, by solid-state gating, by modifying the magnetic anisotropy to $K_{S_{E \neq 0}}$. In region 1, an AC field located 1.2 μ m away from the left edge of the waveguide is responsible for exciting SWs propagating to the left ($-x$) and right ($+x$) directions. The SWs traveling to the right first encounter region 2 and finally propagate to region 3, where we detect the SWs after scattering twice at the entry and exit of region 2 due to the modified SA $K_{S_{E \neq 0}}$ in that region. The SW propagating to the left of the waveguide is absorbed due to the exponentially increasing α , which prevents SW reflection at the left edge.

In this article, data are extracted by defining a row of cells of $2 \times 2 \times 2.5$ nm at the top surface of the strip along the x direction of the strip, centered around $y = 32$ nm (see Figure 1b). As the spin-wave profile is uniform across the thickness, we choose this region to minimize simulation time, saving only data from the selected region. The region is selected around the center of the strip to avoid peculiarities in the demagnetizing field due to edge effects. A Fast Fourier Transform (FFT) in space and time of the dynamic magnetization m_x component in this box allows us to obtain the dispersion relation of our system as shown in Figure 2a. The highest intensity of the FFT follows very closely the analytical dispersion (shown by the red dashed line) as given by⁴²

$$f = \frac{\mu_0 \gamma}{2\pi} \sqrt{\left(H + \frac{2A_{ex}}{\mu_0 M_S} k^2 \right) \left(H + \frac{2A_{ex}}{\mu_0 M_S} k^2 + M_S - H_p(V_{gate}) \right) + \frac{M_S}{4} (1 - e^{-2t|k|}) (M_S - H_p(V_{gate}))}, \quad (1)$$

with H the applied static magnetic field, k the SW wavevector and $H_p(V_{gate})$ the voltage (V_{gate}) dependent out-of-plane SA field. From this excellent correspondence, we conclude that our Micromagnetic simulation setup correctly describes DE-mode SWs in Co-based thin films. Once the SWs are excited in region 1, they propagate to region 2, at the center of the strip, where the effective $K_{S_{E \neq 0}}$ is modified to reproduce the VCMA effect induced at the interface between the

Co and the MgO. Here, we include the VCMA effect as a linear dependency on the applied electric field⁴³. The voltage-dependent out-of-plane SA $H_p(V_{gate})$ can be expressed as $\beta \frac{2K_S}{\mu_0 M_S t_{Co}}$ where β is a linear term with V_{gate} describing the effect of the electric field on the change of K_S and t_{Co} the thickness of the Co layer. Here, we have used the value based on the work of Kasukawa *et al.* multiplied by ten to boost

the effect in our simulations, which corresponds to a relative change of the total perpendicular magnetic anisotropy of 0.44%. Once the SWs leave region 2, they are detected in region 3, where the anisotropy is set to $K_{S_{E=0}}$ as in region 1. In our following simulations, we vary the gate width (W_{gate}) from 0 to $2.5 \mu\text{m}$, and K_S is increased (resp. decreased) by a maximum amount of 3 mJ/m^2 .

The effect of the change of K_S can be understood from the inset of Figure 2a, which shows a change in the dispersion, under the gated region, for different K_S . Once K_S is increased by $+\Delta K_S$ (resp. decreased by $-\Delta K_S$), the dispersion relation is shifted down (resp. up). Let us now assume a SW excited with a wavevector $k = 5 [2\pi \text{ rad}/\mu\text{m}]$. An increase of anisotropy $+\Delta K_S$ (resp. decrease of anisotropy $-\Delta K_S$) will result in a scattering of the SW to a wavevector k_2 (resp. k_1). By numerically solving equation 1 for the wavevector k , we plot, in fig. 2b, the change of wavevector $\Delta k = |k_{0\%} - k_{-0.44\%}|$ with $k_{0\%}$ the initial SA and $k_{-0.44\%}$ the SA corresponding to a decrease of 0.44% of $k_{0\%}$. As K_S is an interfacial effect, the VCMA effect scales as $1/t_{Co}$. The dependency of Δk with increasing frequency can be understood via its dispersion relation. For all thicknesses, Δk increases with frequency, which is a direct consequence of the flattening of the dispersion relation at higher frequencies (e.g., Fig 2a), which increases the change in Δk for a given change in K_S . The consequence of a change of wavevector is a phase shift of the propagating SW induced in the gated region. Therefore, an increase (decrease) of SA results in a decrease (increase) of wavevector, inducing a positive phase shift due to its higher (lower) group velocity (v_g). Hence, we conclude that, in accordance with the analytical dispersion, the total amount of acquired phase shift per unit length (due to the Δk) of a SW traveling through the gated region 2 strongly depends on the conduit layer thickness via its dispersion.

Figure 3a shows the normalized M_x/M_S component of the magnetization along the x -axis of the waveguide. To compare our results, we choose the same time instant of the M_x/M_S component, corresponding to the last time frame of the simulation ($t = 10 \text{ ns}$). This ensures that the amplitude of M_x/M_S over time does not vary and corresponds to the magnetization equilibrium. As described previously, an exponential damping profile is present at both ends of the waveguide, delimited by the black dashed lines (see Fig.3a). As seen in Figure 3a, the SW is excited $1.2 \mu\text{m}$ from the left side of the strip, noted by a red dashed line. The two continuous black lines centered around the strip indicate the gated region with a width of $W_{gate} = 1.1 \mu\text{m}$. The amplitude of M_x/M_S shows the typical exponential decay with distance due to damping. Once K_S is decreased (resp. increased) by a factor $-\Delta K_S$ (resp. $+\Delta K_S$) in the gated region as shown by the blue curves, a positive (resp. negative) phase shift is induced in the gated region, which, after traveling into region 2, results in a constant phase shifted propagating SW that can be measured in region 3. Due to the small change in k , no significant back-scatter effects are observed at the interfaces between regions 1 and 2 and region 2 and 3. This simple representation captures, in essence, the effect of VCMA on the phase change of the SWs. On the other hand, using these profiles, we can extract the effect of

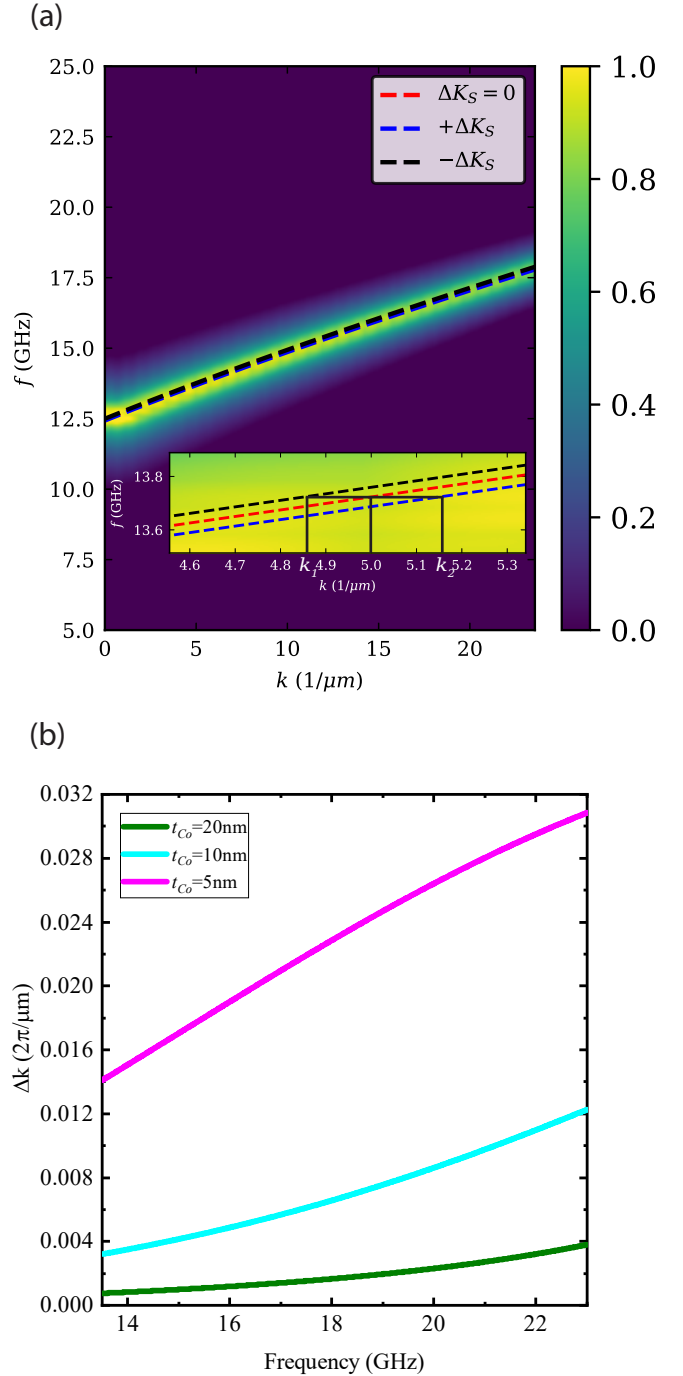


FIG. 2: (a) FFT of M_x/M_S component of Micromagnetic simulation for a $\text{Co}(t_{Co} = 5 \text{ nm})$ waveguide. The inset shows the effect of a change of K_S on the dispersion from equation 1. (b) Numerically deduced change of wavevector due to the VCMA as a function of frequency for $t_{Co} = 5, 10, \text{ and } 20 \text{ nm}$ waveguides using equation 1.

gating on the SW attenuation length l_{att} as a function of the frequency for different t_{Co} , as shown in Fig. 3b. To do so, we fit the M_x/M_S component of the magnetization along the x

with the expression

$$A e^{-l_{att}x} \sin(kx + \phi), \quad (2)$$

with A the amplitude, l_{att} the attenuation length, x the position along the x -axis of the waveguide, k the wavevector and ϕ the phase of the SW. As expected, l_{att} decreases with increasing frequency as the dispersion relation flattens off, resulting in a lower v_g . Moreover, the thinner the Co layer, the lower v_g in the studied frequency regime, resulting in a smaller attenuation length. Hence, as the SW phase accumulates with the distance traveled, one must carefully balance the attenuation length and accumulated phase shift per unit length.

In order to extract the accumulated phase of the propagating SW in region 3, resulting from the local VCMA-induced change of wavevector in region 2, we use equation 2 to fit the portion of the SW in region 3 of interest. Here we define the phase shift as $\Delta\phi_{+-} = |\phi_{0\%} - \phi_{\pm 0.44\%}|$ i.e., the difference between the phase of the SW with wavevectors $k_{0\%}$ and $k_{+0.44\%}$ and $k_{0\%}$ and $k_{-0.44\%}$. To compensate for the thickness-dependent change in accumulated phase due to the change in v_g , in Fig. 4 we plot, Δk multiplied by the wavevector-dependent v_g as extracted from the dispersion relation. As expected from the model from equation 1, the VCMA-induced phase shift scales linearly with the change of K_S . Moreover, we identify the necessity to multiply the phase by the v_g in order for the accumulated phase to scale as $1/t_{Co}$. This suggests an effect of VCMA on the phase inversely proportional to v_g , implying a time-dependent effect of VCMA on the propagating SW, in the gated region.

Performing full logic operations with SWs requires a π rad shift of the SW compared to a given SW reference signal. Although t_{Co} can be reduced to boost the VCMA effect and, therefore, the phase shift, a reduction in thickness is limited in its efficiency due to the decreased l_{att} . Fig. 5a shows the phase shift $\Delta\phi = |\phi_{0\%} - \phi_{-0.44\%}|$ as a function of the gate length for wavevectors of 5.84, 8.35, and 10.51 [2π rad/ μ m] for a Co layer of $t_{Co} = 5$ nm. As expected from the analytical model from equation 1, we observe a linear increase of the $\Delta\phi$ with increasing W_{gate} . Good correspondence between the analytical model ($\Delta k \times W_{gate}$) and the simulations show that the analytical model can accurately predict phase changes induced by VCMA.

To gain further insight into the frequency dependency of the VCMA effect, we plot the $\Delta\phi$ as a function of the SW frequency in Fig. 5b. Indeed, as v_g decreases with SW frequency and Co layer thickness, the accumulated phase increases for a given W_{gate} . A discrepancy between the Micro-magnetic and analytical model is observed for lower wavevector (open symbols) and is currently speculatively attributed to reflections and/or finite size effect of the simulation box which becomes of the order of the SW wavelength. The linear trend in the VCMA-dependent $\Delta\phi$ with the excitation frequency and W_{gate} allows for a discussion of the feasibility of a π rad phase shift induced by a local changes of K_S for the application of logic operation. Let us assume, as an example, a wavevector $k = 8.35$ [2π rad/ μ m] and W_{gate} of 1.5 μ m. Assuming minimum reflections from the gated area and no resonance in the gated region due to the SW wavelength being

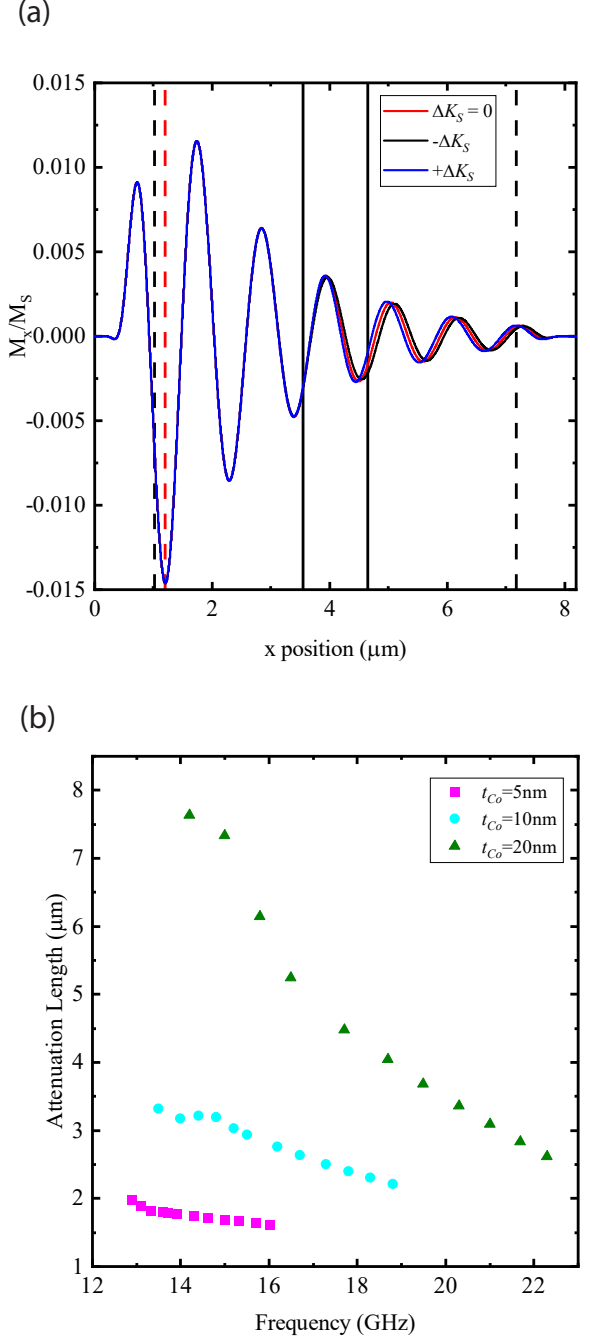


FIG. 3: (a) M_x/M_S component of the magnetization along x at time instant $t = 10$ ns for a $t_{Co} = 5$ nm layer for no change of anisotropy in red, a positive change in blue and a negative change in black. Numbers 1, 2, and 3 correspond, respectively, to regions 1, 2, and 3 shown in Fig. 1 with the region 2 delimited by the 2 continuous black lines. (b) Fitted attenuation length l_{att} ($t = 10$ ns) as a function of frequency excitation of SWs for $t_{Co} = 5, 10,$ and 20 nm.

commensurable with the gated region width, we can naively deduce, from Figure 5a, that the maximum possible achiev-

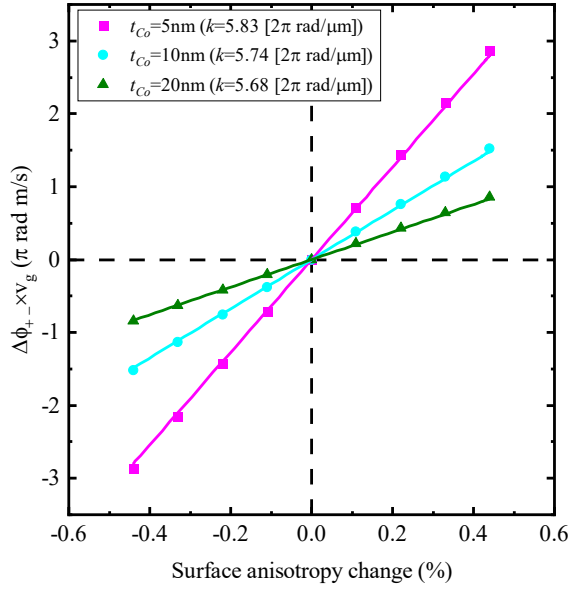


FIG. 4: Phase shift ($t = 10$ ns) multiplied by the frequency-dependent v_g as a function of K_S change for $t_{Co} = 5, 10,$ and 20 nm from Micromagnetic simulations (symbols) and analytical model (continuous lines).

able $\Delta\phi$, in these conditions, is of the order of 12.6 [π mrad] when using a MgO dielectric as a catalyst for the change of K_S . As the changes of SA, in this work, were assumed to be Kasukawa *et.al.* multiplied by ten to boost the effect in our simulations, a $\Delta\phi$ of 1.26 [π mrad] can be expected for a realistic, non-boostered, VCMA-induced K_S change. It is important to note that as a positive change of K_S will induce an additional $\Delta\phi$ of 1.26 [π mrad] due to the symmetrical $\Delta\phi$ induced by a change of SA, the total $\Delta\phi$, in these conditions, would be 2.5 [π mrad]. While we think this phase change is commensurable with the limit of phase sensitivity of all-electrical propagating SW spectroscopy measurement methods⁴⁴, an optimization of the excitation frequency and W_{gate} is needed to achieve phase changes of the order of π rad phase shift. Although MgO does not allow for significant changes of K_S , optimizing the dielectric layer may considerably increase the efficiency of VCMA-induced $\Delta\phi$ with DE SWs. One possibility is the use of a GdO_x dielectric, which showed an efficiency of change of K_S of the order of 500 $fJ/(V \cdot m)$ at Co($t_{Co}=0.9$ nm)/GdO_x($t_{GdO}=3$ nm) interfaces⁴⁵. This efficiency in VCMA is 200 times superior to MgO, which could potentially increase the $\Delta\phi$ to a value of 0.25 [π rad]. By tuning the applied voltage within the breakdown limit of GdO_x and optimizing the excitation frequency and W_{gate} , we could, therefore, imagine further improvement in the efficiency of the $\Delta\phi$. However, the use of GdO_x presents a significant limitation in time efficiency due to the oxidation mechanism responsible for the change of K_S . On top of tuning the parameters previously described, the efficiency of VCMA of $\Delta\phi$ is also shown to scale as $1/t_{Co}$, meaning that a thinner layer would

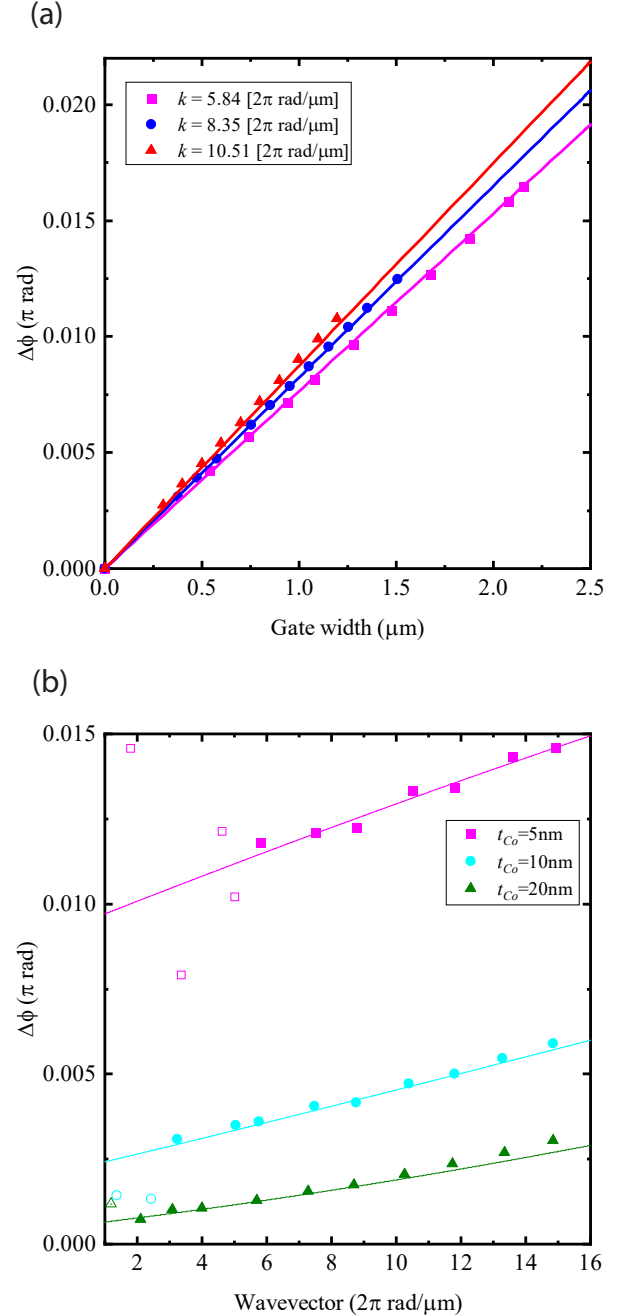


FIG. 5: (a) Phase shift ($t = 10$ ns) as a function of the W_{gate} for a $t_{Co} = 5$ nm waveguide and wavevectors $5.84, 8.35,$ and 10.51 [2π rad/ μ m] as obtained from Micromagnetic simulations (symbols) and analytical model (solid lines). (b) Phase shift ($t = 10$ ns) as a function of the SW wavevector for a $t_{Co} = 5$ nm waveguide from Micromagnetic simulations (symbols) and analytical model (solid lines). A discrepancy between the Micromagnetics and analytical model is observed for lower wavevector as denoted by the open symbols.

improve further the efficiency of VCMA and get closer to a π rad phase shift. It is important to note that the effect of VCMA on interfacial Dzyaloshinskii-Moriya interaction (iDMI) has not been included in this study, but further research in the combination of VCMA effect on K_S and iDMI may lead to even more significant changes of phase as VCMA effect have been reported on iDMI³⁹.

In summary, we have investigated the effect of a local change of K_S on the phase of propagating SWs in the DE configuration. We have shown a linear dependency of the VCMA-induced $\Delta\phi$ with the excitation frequency and W_{gate} in accordance with analytical models. Moreover, we showed the importance of the v_g in the expected $\Delta\phi$ when studying the effect of a change of t_{Co} . We determined that the maximum realistic $\Delta\phi$ in Co($t_{Co}=5\text{nm}$)/MgO stack is of the order of 2.5 [π mrad] and can be further improved by increasing the frequency excitation, W_{gate} , decreasing t_{Co} and by opting for a GdO_x dielectric, the latter allowing to improve the efficiency of change of phase by a factor 200 compared to what can be expected from a MgO dielectric.

ACKNOWLEDGMENTS

This project has received funding from the European Union's Horizon 2020 research and innovation programme under the Marie Skłodowska-Curie grant agreement No. 860060 "Magnetism and the effect of Electric Field" (Mag-nEFi).

DATA AVAILABILITY STATEMENT

The data that support the findings of this study are available from the corresponding author upon reasonable request.

- ¹A. V. Chumak, V. I. Vasyuchka, A. A. Serga, and B. Hillebrands, "Magnon spintronics," *Nature Physics* **11**, 453–461 (2015).
- ²V. V. Kruglyak, S. O. Demokritov, and D. Grundler, "Magnonics," *Journal of Physics D: Applied Physics* **43**, 260301 (2010).
- ³A. V. Chumak, A. A. Serga, and B. Hillebrands, "Magnonic crystals for data processing," *Journal of Physics D: Applied Physics* **50**, 244001 (2017).
- ⁴S. O. Demokritov, A. A. Serga, A. André, V. E. Demidov, M. P. Kostylev, B. Hillebrands, and A. N. Slavin, "Tunneling of dipolar spin waves through a region of inhomogeneous magnetic field," *Phys. Rev. Lett.* **93**, 047201 (2004).
- ⁵A. V. Chumak, V. S. Tiberkevich, A. D. Karenowska, A. A. Serga, J. F. Gregg, A. N. Slavin, and B. Hillebrands, "All-linear time reversal by a dynamic artificial crystal," *Nature Communications* **1**, 141 (2010).
- ⁶K. Vogt, F. Y. Fradin, J. E. Pearson, T. Sebastian, S. D. Bader, B. Hillebrands, A. Hoffmann, and H. Schultheiss, "Realization of a spin-wave multiplexer," *Nature Communications* **5**, 3727 (2014).
- ⁷M. Vogel, A. V. Chumak, E. H. Waller, T. Langner, V. I. Vasyuchka, B. Hillebrands, and G. von Freymann, "Optically reconfigurable magnetic materials," *Nature Physics* **11**, 487–491 (2015).
- ⁸M. Vogel, R. Alßmann, P. Pirro, A. V. Chumak, B. Hillebrands, and G. von Freymann, "Control of Spin-Wave propagation using magnetisation gradients," *Scientific Reports* **8**, 11099 (2018).
- ⁹E. Albiseti, S. Tacchi, R. Silvani, G. Scaramuzzi, S. Finizio, S. Wintz, C. Rinaldi, M. Cantoni, J. Raabe, G. Carlotti, R. Bertacco, E. Riedo, and D. Petti, "Optically inspired nanomagnonics with nonreciprocal spin waves in synthetic antiferromagnets," *Adv Mater* **32**, e1906439 (2020).
- ¹⁰Z. Wang, Y. Sun, M. Wu, V. Tiberkevich, and A. Slavin, "Control of spin waves in a thin film ferromagnetic insulator through interfacial spin scattering," *Phys. Rev. Lett.* **107**, 146602 (2011).
- ¹¹C. Liu, S. Wu, J. Zhang, J. Chen, J. Ding, J. Ma, Y. Zhang, Y. Sun, S. Tu, H. Wang, P. Liu, C. Li, Y. Jiang, P. Gao, D. Yu, J. Xiao, R. Duine, M. Wu, C.-W. Nan, J. Zhang, and H. Yu, "Current-controlled propagation of spin waves in antiparallel, coupled domains," *Nature Nanotechnology* **14**, 691–697 (2019).
- ¹²M. S. Sarker, L. Yao, H. Yamahara, K. Ma, Z. Liao, K. Terao, S. Tang, S. G. Ramaraj, M. Seki, and H. Tabata, "Reconfigurable magnon interference by on-chip dynamic wavelength conversion," *Scientific Reports* **13**, 4872 (2023).
- ¹³T. Schneider, A. A. Serga, B. Leven, B. Hillebrands, R. L. Stamps, and M. P. Kostylev, "Realization of spin-wave logic gates," *Applied Physics Letters* **92**, 022505 (2008), https://pubs.aip.org/aip/apl/article-pdf/doi/10.1063/1.2834714/14386766/022505_1_online.pdf.
- ¹⁴K.-S. Lee and S.-K. Kim, "Conceptual design of spin wave logic gates based on a Mach-Zehnder-type spin wave interferometer for universal logic functions," *Journal of Applied Physics* **104**, 053909 (2008), https://pubs.aip.org/aip/jap/article-pdf/doi/10.1063/1.2975235/15020378/053909_1_online.pdf.
- ¹⁵A. Khitun, M. Bao, and K. L. Wang, "Magnonic logic circuits," *Journal of Physics D: Applied Physics* **43**, 264005 (2010).
- ¹⁶F. Matsukura, Y. Tokura, and H. Ohno, "Control of magnetism by electric fields," *Nature Nanotechnology* **10**, 209–220 (2015).
- ¹⁷M. Weisheit, S. Fähler, A. Marty, Y. Souche, C. Poinsignon, and D. Givord, "Electric field-induced modification of magnetism in thin-film ferromagnets," *Science* **315**, 349–351 (2007), <https://www.science.org/doi/pdf/10.1126/science.1136629>.
- ¹⁸M. Endo, S. Kanai, S. Ikeda, F. Matsukura, and H. Ohno, "Electric-field effects on thickness dependent magnetic anisotropy of sputtered MgO/Co40Fe40B20/Ta structures," *Applied Physics Letters* **96**, 212503 (2010), https://pubs.aip.org/aip/apl/article-pdf/doi/10.1063/1.3429592/13413496/212503_1_online.pdf.
- ¹⁹C. Bi, Y. Liu, T. Newhouse-Illige, M. Xu, M. Rosales, J. W. Freeland, O. Mryasov, S. Zhang, S. G. E. te Velthuis, and W. G. Wang, "Reversible control of co magnetism by voltage-induced oxidation," *Phys. Rev. Lett.* **113**, 267202 (2014).
- ²⁰Y. Hibino, T. Koyama, A. Obinata, T. Hirai, S. Ota, K. Miwa, S. Ono, F. Matsukura, H. Ohno, and D. Chiba, "Peculiar temperature dependence of electric-field effect on magnetic anisotropy in Co/Pd/MgO system," *Applied Physics Letters* **109**, 082403 (2016), https://pubs.aip.org/aip/apl/article-pdf/doi/10.1063/1.4961621/14484853/082403_1_online.pdf.
- ²¹Y. Shiota, T. Nozaki, F. Bonell, S. Murakami, T. Shinjo, and Y. Suzuki, "Induction of coherent magnetization switching in a few atomic layers of FeCo using voltage pulses," *Nature Materials* **11**, 39–43 (2012).
- ²²D. Chiba, S. Fukami, K. Shimamura, N. Ishiwata, K. Kobayashi, and T. Ono, "Electrical control of the ferromagnetic phase transition in cobalt at room temperature," *Nature Materials* **10**, 853–856 (2011).
- ²³W.-G. Wang, M. Li, S. Hageman, and C. L. Chien, "Electric-field-assisted switching in magnetic tunnel junctions," *Nature Materials* **11**, 64–68 (2012).
- ²⁴T. Maruyama, Y. Shiota, T. Nozaki, K. Ohta, N. Toda, M. Mizuguchi, A. A. Tulapurkar, T. Shinjo, M. Shiraishi, S. Mizukami, Y. Ando, and Y. Suzuki, "Large voltage-induced magnetic anisotropy change in a few atomic layers of iron," *Nature Nanotechnology* **4**, 158–161 (2009).
- ²⁵U. Bauer, L. Yao, A. J. Tan, P. Agrawal, S. Emori, H. L. Tuller, S. van Dijken, and G. S. D. Beach, "Magneto-ionic control of interfacial magnetism," *Nature Materials* **14**, 174–181 (2015).
- ²⁶B. Dieny and M. Chshiev, "Perpendicular magnetic anisotropy at transition metal/oxide interfaces and applications," *Rev. Mod. Phys.* **89**, 025008 (2017).
- ²⁷H. X. Yang, M. Chshiev, B. Dieny, J. H. Lee, A. Manchon, and K. H. Shin, "First-principles investigation of the very large perpendicular magnetic anisotropy at fe|mgo and co|mgo interfaces," *Phys. Rev. B* **84**, 054401 (2011).
- ²⁸C.-G. Duan, J. P. Velev, R. F. Sabirianov, Z. Zhu, J. Chu, S. S. Jaswal, and E. Y. Tsymlal, "Surface magnetoelectric effect in ferromagnetic metal films," *Phys. Rev. Lett.* **101**, 137201 (2008).

- ²⁹K. Nakamura, R. Shimabukuro, Y. Fujiwara, T. Akiyama, T. Ito, and A. J. Freeman, "Giant modification of the magnetocrystalline anisotropy in transition-metal monolayers by an external electric field," *Phys. Rev. Lett.* **102**, 187201 (2009).
- ³⁰M. Tsujikawa and T. Oda, "Finite electric field effects in the large perpendicular magnetic anisotropy surface Pt/Fe/Pt(001): A first-principles study," *Phys. Rev. Lett.* **102**, 247203 (2009).
- ³¹S. Miwa, M. Suzuki, M. Tsujikawa, K. Matsuda, T. Nozaki, K. Tanaka, T. Tsukahara, K. Nawaoka, M. Goto, Y. Kotani, T. Ohkubo, F. Bonell, E. Tamura, K. Hono, T. Nakamura, M. Shirai, S. Yuasa, and Y. Suzuki, "Voltage controlled interfacial magnetism through platinum orbits," *Nature Communications* **8**, 15848 (2017).
- ³²Q. Wang, A. V. Chumak, L. Jin, H. Zhang, B. Hillebrands, and Z. Zhong, "Voltage-controlled nanoscale reconfigurable magnonic crystal," *Phys. Rev. B* **95**, 134433 (2017).
- ³³B. Rana and Y. Otani, "Voltage-controlled reconfigurable spin-wave nanochannels and logic devices," *Phys. Rev. Appl.* **9**, 014033 (2018).
- ³⁴V. N. Krivoruchko, A. S. Savchenko, and V. V. Kruglyak, "Electric-field control of spin-wave power flow and caustics in thin magnetic films," *Phys. Rev. B* **98**, 024427 (2018).
- ³⁵X.-g. Wang, L. Chotorlishvili, G.-h. Guo, and J. Berakdar, "Electric field controlled spin waveguide phase shifter in YIG," *Journal of Applied Physics* **124**, 073903 (2018), https://pubs.aip.org/aip/jap/article-pdf/doi/10.1063/1.5037958/15214574/073903_1_online.pdf.
- ³⁶X. Zhang, T. Liu, M. E. Flatté, and H. X. Tang, "Electric-field coupling to spin waves in a centrosymmetric ferrite," *Phys. Rev. Lett.* **113**, 037202 (2014).
- ³⁷A. S. Tatarenko, G. Srinivasan, and M. I. Bichurin, "Magnetolectric microwave phase shifter," *Applied Physics Letters* **88**, 183507 (2006), https://pubs.aip.org/aip/apl/article-pdf/doi/10.1063/1.2198111/14659002/183507_1_online.pdf.
- ³⁸S. Kasukawa, Y. Shiota, T. Moriyama, and T. Ono, "Evaluation of electric field effect on interface magnetic properties by propagating spin wave in pt/co/mgo structures," *Japanese Journal of Applied Physics* **57**, 080309 (2018).
- ³⁹K. Nawaoka, S. Miwa, Y. Shiota, N. Mizuochi, and Y. Suzuki, "Voltage induction of interfacial dzyaloshinskii–moriya interaction in au/fe/mgo artificial multilayer," *Applied Physics Express* **8**, 063004 (2015).
- ⁴⁰K. Nawaoka, Y. Shiota, S. Miwa, H. Tomita, E. Tamura, N. Mizuochi, T. Shinjo, and Y. Suzuki, "Voltage modulation of propagating spin waves in Fe," *Journal of Applied Physics* **117**, 17A905 (2015), https://pubs.aip.org/aip/jap/article-pdf/doi/10.1063/1.4914060/14776090/17a905_1_online.pdf.
- ⁴¹A. Vansteenkiste, J. Leliaert, M. Dvornik, M. Helsen, F. Garcia-Sanchez, and B. Van Waeyenberge, "The design and verification of MuMax3," *AIP Advances* **4**, 107133 (2014), https://pubs.aip.org/aip/adv/article-pdf/doi/10.1063/1.4899186/12878560/107133_1_online.pdf.
- ⁴²S. Choudhury, A. K. Chaurasiya, A. K. Mondal, B. Rana, K. Miura, H. Takahashi, Y. Otani, and A. Barman, "Voltage controlled on-demand magnonic nanochannels," *Science Advances* **6**, eaba5457 (2020), <https://www.science.org/doi/pdf/10.1126/sciadv.aba5457>.
- ⁴³C. Song, B. Cui, F. Li, X. Zhou, and F. Pan, "Recent progress in voltage control of magnetism: Materials, mechanisms, and performance," *Progress in Materials Science* **87**, 33–82 (2017).
- ⁴⁴M. Bailleul, D. Olligs, and C. Fermon, "Propagating spin wave spectroscopy in a permalloy film: A quantitative analysis," *Applied Physics Letters* **83**, 972–974 (2003), https://pubs.aip.org/aip/apl/article-pdf/83/5/972/7457819/972_1_online.pdf.
- ⁴⁵U. Bauer, L. Yao, A. J. Tan, P. Agrawal, S. Emori, H. L. Tuller, S. van Dijken, and G. S. D. Beach, "Magneto-ionic control of interfacial magnetism," *Nature Materials* **14**, 174–181 (2015).
- ⁴⁶L. Herrera Diez, D. Chiba, D. A. Gilbert, S. Granville, and K. Leistner, "Magneto-ionic and electrostatic gating of magnetism: Phenomena and devices," *Applied Physics Letters* **123**, 130401 (2023), https://pubs.aip.org/aip/apl/article-pdf/doi/10.1063/5.0176639/18140144/130401_1_5.0176639.pdf.